ARTICLE

Single Nanowire Thermal Conductivity Measurements by Raman Thermography

Gregory S. Doerk, Carlo Carraro, and Roya Maboudian*

Department of Chemical Engineering, University of California, Berkeley, California 94720

ABSTRACT A facile, rapid, and nondestructive technique for determining the thermal conductivity of individual nanowires based on Raman temperature mapping has been demonstrated. Using calculated absorption efficiencies, the thermal conductivities of single cantilevered Si nanowires grown by the vapor–liquid–solid method are measured and the results agree well with values predicted by diffuse phonon boundary scattering. As a measurement performed on the wire, thermal contact effects are avoided and ambient air convection is found to be negligible for the range of diameters measured. The method's versatility is further exemplified in the reverse measurement of a single nanowire absorption efficiency assuming diffuse phonon boundary scattering. The results presented here outline the broad utility that Raman thermography may have for future thermoelectric and photovoltaic characterization of nanostructures.

KEYWORDS: silicon · Raman spectroscopy · thermal characterization · optical absorption · nanowire · vapor–liquid–solid · photovoltaic

Many interesting and potentially useful properties of semiconductor nanowires (NWs) stem from the parity of their confined dimension (the diameter) with important nanometer-scale characteristic lengths. For example, silicon nanowires with diameters on the order of their phonon mean free paths or less exhibit suppressed thermal conductivities due to phonon boundary scattering.[1] Surface roughening may diminish Si NW thermal conductivities even further, introducing the possibility of viable silicon thermoelectric devices.[2] In another exemplary case, the dielectric mismatch between a NW and its surrounding medium gives rise to resonant interactions with electromagnetic radiation when the wavelength of the incident field is commensurate with the radial dimension of the NW.[3] These optical antenna effects result in optical absorption resonances,[3–5] large polarization anisotropies,[6] and enhanced Raman scattering[7] with sensitivity to radial composition gradients.[8]

Despite recent advances in the understanding of nanowire (NW) properties, the development of NW-based technologies is hindered by a lack of rapid, nondestructive characterization methods with submicrometer resolution. In the measurement of NW and nanotube thermal conductivity, precise measurement methods based on microheating[1,9] and the 3ω technique[10] have been developed. However, these techniques require carefully microfabricated devices, and the NW must be suspended across the device—a process that is often slow and tedious and is essentially destructive. Interfacial contact resistances can also result in a potentially significant source of error for these methods, especially for large diameter NWs.[9] As a noncontact probe of local temperature with submicrometer resolution, Raman thermometry is especially suited for measuring nanostructure thermal properties and has recently been applied to graphene[11] and carbon nanotube bundles.[12] In such a method, optical absorption of the material at the relevant wavelength must be independently measured or estimated.

In this paper, we present a simple, noncontact method to measure the thermal conductivity of cantilevered NWs by locally heating them along their axes with a focused laser while simultaneously measuring the local temperature at the same spot through Raman spectrometry. Optical absorption is calculated using a solution to Maxwell's equations for an infinite dielectric cylinder and is validated by the good agreement of the extracted thermal conductivities with those expected due to diffuse phonon boundary scattering. By comparing results performed at reduced pressure to those done in air, we find that convection does not induce significant error for the range of diameters probed. Finally, we note that if a functional relation-

*Address correspondence to maboudia@berkeley.edu.

Received for review June 2, 2010 and accepted July 9, 2010.

Published online July 22, 2010. 10.1021/nn1012429

ship for thermal conductivity is known, this method introduces a simple way to directly measure optical absorption cross sections.

RESULTS AND DISCUSSION

Figure 1a shows a top view schematic of the measurement setup. A Raman map is made around a cantilevered Si NW (an example is shown in Figure 1b) by moving the sample with respect to the laser spot using a nanopositioning stage. The laser heats the NW at a length from the trench wall, L, where it crosses the NW axis. In Raman spectra of crystals, the position of phonon lines depends on temperature as a result of anharmonicity in the vibrational potential energy. Thus, temperature can be measured locally at the same laser spot by the position of the optical phonon peak in the acquired Raman spectra. For Si NWs with diameters as small as 30 nm and for the temperature range of 20 to 300 °C, the peak position depends linearly on temperature and matches the same dependence found in bulk Si. Therefore, we use the bulk Si temperature dependence for Si optical phonon frequency ($d\omega/dT = -0.022 \pm 0.001$ cm^{-1} °C^{-1}).[13] The trench wall acts as a thermal sink maintaining constant (room) temperature, and the heat transfer problem is effectively one-dimensional for two reasons: First, in cases where the effective phonon mean free path for heat transfer in bulk crystals (on the order of a few 100 nm for Si at room temperature[14]) is expected to be larger than the relevant sample dimension, it may not be possible for a temperature gradient to exist across this dimension.[15] This is true for Si NWs with diameters in the range studied here. The axial dimensions are much longer than the same effective phonon mean free path, making local temperature definition unproblematic along NW lengths. Second, since the laser spot diameter is much larger than the NW diameter, the measured temperature can be considered radially averaged and the heat problem is rendered one-dimensional.

Radiative heat loss is negligible compared with conduction near room temperature.[9,12] In the simplest case where convection may also be neglected, the problem may be treated with a simple linear heat resistor model. At steady state under these conditions, the temperature will be constant from the laser spot to the end of the NW (opposite side from the NW base). Then the temperature difference is given by

$$\Delta T = \left(R_c + \frac{4L}{\pi D_w^2 k_w}\right)\dot{Q} \qquad (1)$$

where $\dot{Q}$ is the heat conducted down the wire, D_w is the NW diameter, R_c is the thermal contact resistance at the NW base, k_w is the NW thermal conductivity, and ΔT is the difference between the radially averaged temperature at the laser spot L and the temperature at the NW base ($\Delta T = \bar{T} - T_o$). Considering that ΔT increases

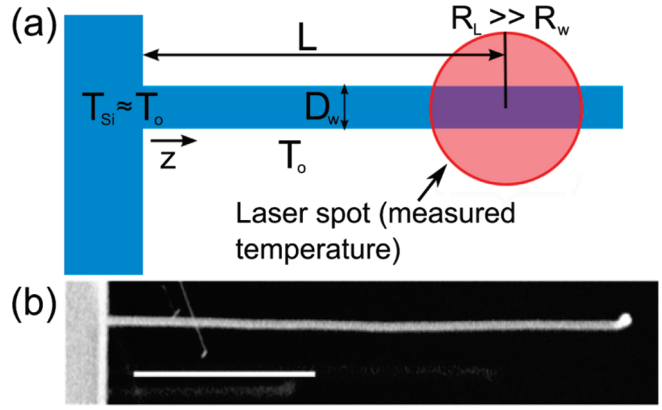

Figure 1. (a) Schematic (top view) of the measurement principle. (b) SEM image of an as-grown cantilever Si NW (scale bar = 5 μm).

linearly with L, we may instead measure the slope S of ΔT *versus* L (determined by linear regression) and rearrange (1) to develop a simple expression for thermal conductivity that bypasses a dependence on the thermal contact resistance as well as any effect from the uncertainty in the absolute magnitude of L:

$$k_w = \frac{4\dot{Q}}{\pi D_w^2 S} \qquad (2)$$

If we assume that all of the laser power absorbed is converted to heat that is conducted down the wire, then $\dot{Q}$ is proportional to the laser power at the sample (P) and the ratio of NW area exposed to the beam to the area of the focused beam spot. Using an average laser power is appropriate since the full laser spot diameter is sampled along the length of NW directly under the beam. Approximating the exposed area as $\pi D_w D_L/2$, where D_L is the laser spot diameter, the NW thermal conductivity may be expressed as

$$k_w = \frac{8cQ_aP}{\pi S D_w D_L} \qquad (3)$$

The parameter c is a correction factor that represents the proportion of incident radiation transmitted (not extinguished) with a window in place that was necessary when low pressure measurements were performed to examine the assumption of negligible convection. At low pressure ($<10^{-1}$ Torr), the mean free path of air molecules is over 1000 times larger than the NW diameters, and convection is negligible.[12] This is not necessarily true at ambient pressure. The value of c was estimated by measuring Raman spectra of bulk Si(111) substrates with and without the window in place. Given the small frequency change in the Raman scattered light from the incident light in comparison to the frequency of the incident radiation, the window likely extinguishes incident and scattered radiation almost equally. Since the window extinguishes light twice for Raman spectra collected with the window in place, we obtained a value of c estimated at 0.47 ± 0.02 from the square root of the relative intensities of bulk Si Raman

spectra with and without the window in place. A more detailed explanation for how c is estimated is given in the Supporting Information.

The most important parameter in eq 3 is the absorption efficiency, Q_a, defined as the ratio of the absorption cross section to the geometrically obstructed area.[16] As noted in the beginning of this article, the subwavelength dimensions of NWs result in diameter-dependent modulations in their interactions with light from their dielectric mismatch with the environment. In particular, light absorption resonances arise when the wavelength is matched to an eigenmode of the nanowire.[3,6] Accurate calculation of these resonances may be performed using finite difference techniques,[4,5] but in simple cases, a more computationally friendly approach is to solve for Q_a using Mie-type solutions to Maxwell's equations, which have been shown to describe the diameter and incident wavelength-dependent optical behavior of NWs very well both in Raman spectra[6−8] and photocurrent measurements.[3−5] For radiation at normal incidence polarized along the NW axis (TM polarization), the absorption efficiency for an infinite circular dielectric cylinder can be calculated using the following equation:[16]

$$Q_a = \frac{2}{\alpha}\left[Re\left(B_0 + 2\sum_{n=1}^{\infty} B_n\right) - |B_0|^2 - 2\sum_{n=1}^{\infty}|B_n|^2\right] \quad (4)$$

where

$$B_n = \frac{mJ_n(\alpha)J_n'(m\alpha) - J_n(m\alpha)J_n'(\alpha)}{mH_n(\alpha)J_n'(m\alpha) - J_n(m\alpha)H_n'(\alpha)} \quad (5)$$

In these equations, m is the complex index of refraction, J_n is the Bessel function of the first kind, H_n is the Hankel function of the second kind, $\alpha = \pi D_w/\lambda$, where λ is the wavelength of incident light, and prime denotes differentiation with respect to the parenthetical argument. Using complex index of refraction values at λ = 632.8 nm for bulk single-crystal Si,[17] the calculated absorption efficiencies for Si NWs exhibit characteristic resonances at particular diameters, as shown in Figure 2. Implicit in our approach are assumptions that the native oxide layer (~2−3 nm) has only a negligible effect on absorption and that this calculation based on a cylinder works well for Si NWs though their actual radial cross sections are hexagonal.[18] Furthermore, because our NWs exhibit varying degrees of tapering, we use a diameter that is averaged over the probed length, the consequence of which we will discuss later.

Figure 3a is a SEM image of a 78 nm diameter Si NW measured in this study, and Figure 3b is the corresponding Raman intensity map of the same wire in ambient air at a laser power of 0.4 mW. An illustrative Raman spectrum centered on the optical phonon frequency taken at the point marked by a circle in (b) is shown in Figure 3c. This shape is typical for single-

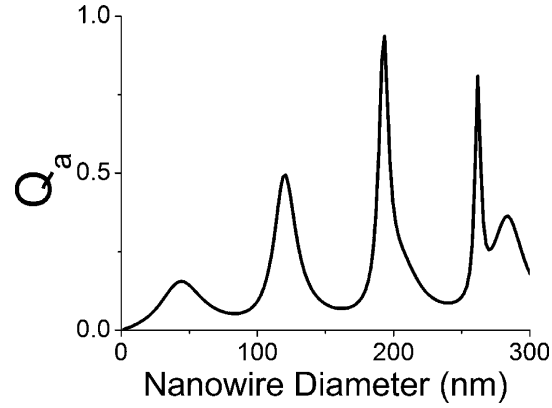

Figure 2. Calculated Si NW absorption efficiencies, Q_a, as a function of diameter using eq 4 in the text.

crystal Si and shows no asymmetric broadening to lower wavenumber that is characteristic of phonon confinement and is usually found only in Si NWs less than ~20 nm in diameter.[19] (Raman mapping under vacuum and selected spectra from this map for this wire—the smallest diameter wire investigated in this report—are given in the Supporting Information.) A line profile of the Raman shift is extracted from the highest intensity vertical line on the Raman map, marked by a black dashed line in Figure 3b, and the temperature increase as a function of L is obtained using the known $d\omega/dT$ value, as shown in Figure 3d. The step size may be made arbitrarily small (limited by the piezoelectric stage resolution) as long as the laser-induced temperature difference increases monotonically along the NW axis and the total temperature increase is greater than the temperature measurement error. Additionally, though the maximum temperature rise does exceed 100 K in some measurements, the thermal conductivity of Si NWs has been found to be very flat in the vicinity of room temperature,[1] indicating that it may be considered constant for this limited temperature range.

The simplicity of both setup and calculation renders the cantilever geometry used here ideal for the measurement of thermal conductivity through combined laser heating and Raman thermography. The normal incidence of the laser is a noteworthy aid in simplifying the calculation; heating with laser light at an oblique incidence requires the inclusion of transverse electric (TE) cross modes in determining the absorption efficiency.[16] In principle, though, Raman thermography may also be applied to nanowires or nanotubes in a variety of in-plane geometries, which are commonly used in many characterization methods. For nanowires in a bridging geometry for instance, the thermal conductivity can be obtained from the curvature of the parabolic temperature−position curve (convection and radiation are asssumed to be negligible). Unfortunately, the thermal contact resistance remains in the expression, adding a level of uncertainty.[20] Typical device geometries (where a NW sits on top of an insulator with

metallic electrical contacts) may also be considered, though a term accounting for heat transfer to the substrate must usually be included in the analysis.[21] Nevertheless, with the precision temperature measurements possible through Raman thermometry, it may be possible in any setup to decompose the heat transfer problem in a way to isolate thermal conductivity, or to study limiting cases such as when thermal contact resistance is negligible, indicating the versatility of Raman thermal measurements. Moreover, Raman thermometry may be used in conjunction with other electrical or optical measurements to reveal concurrent thermal behavior.

In all conditions, care must be taken to distinguish signal from the NW under inspection from other nearby NWs. While the Rayleigh criterion for resolution indicates a minimal in-plane NW separation of approximately half the laser spot size (~0.6 μm here), easy discrimination of the Raman signal from distinct NWs of the same type suggests a practical separation of a couple of micrometers. Additionally, there are possible limitations in the length or diameter of NWs investigated through the technique presented here. While the minimum or maximum NW length is not set by the separation of the contacts (as is the case in the microheater method[9]), the length of the NW must be longer than the laser spot diameter to preclude end effects, and the NW should be long enough so that a temperature−position slope may be obtained with minimal error. However, since the conductive thermal resistance of the NW grows with increasing distance from thermal sink, for large L it may approach equivalence with convective thermal resistance. In the NWs studied here, the length used is also kept to a minimum since the taper of the NW may significantly change the optical absorption behavior across a large L value. Furthermore, in NWs with diameters smaller than those studied here (<~30 nm), measurements are complicated by the inability to actually see the NWs under the optical microscope, the increased likelihood of destroying the NWs with the laser irradiation and other factors such as the effects of phonon confinement on the Raman spectra.[19] However, the fact that the laser is actually *expected* to heat the NW implies that there is no minimal diameter if proper precautions are used.

The results of thermal conductivity measurements on six Si NWs at low pressure and in air are shown in Figure 4. For comparison, we have also included the Si NW thermal conductivities above room temperature (~310 K) previously measured by Li *et al.*[1] through heated Pt microthermometers[9] as well as the expected curve for Si NW thermal conductivity if the only additional factor lowering its value from that of pure bulk Si is fully diffuse phonon boundary scattering. Applying Matthiessen's rule for multiple scattering, the expected NW thermal conductivity is given as

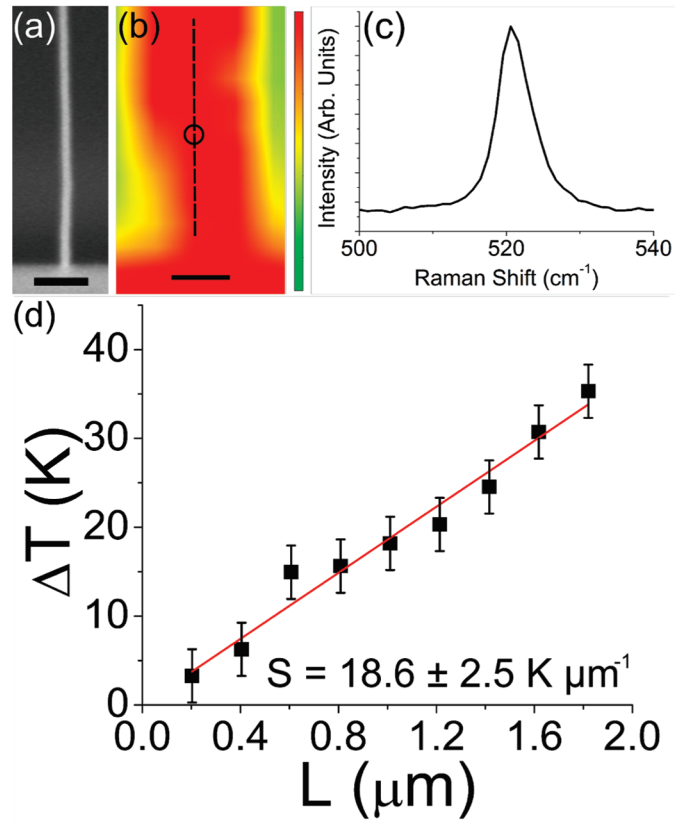

Figure 3. Representative measurement on a single ~78 nm Si NW. SEM image (a) and the corresponding map of the optical phonon integrated peak intensity (b) of this NW. The scale bar is 500 nm for both images. (c) Raman spectrum centered on the optical phonon frequency acquired from the point in (b) marked by a black circle. (d) Temperature difference at the laser spot from the ambient temperature as a function of the distance (L) from the NW−wall contact.

$$k_{w,exp} = \frac{D_w k_{bulk}}{l_{bulk} + D_w} \qquad (6)$$

where k_{bulk} is the bulk Si thermal conductivity (148 W/mK at room temperature) and l_{bulk} is the effective bulk Si mean free path, which is approximately ~300 nm as obtained from measurements on thin films.[14]

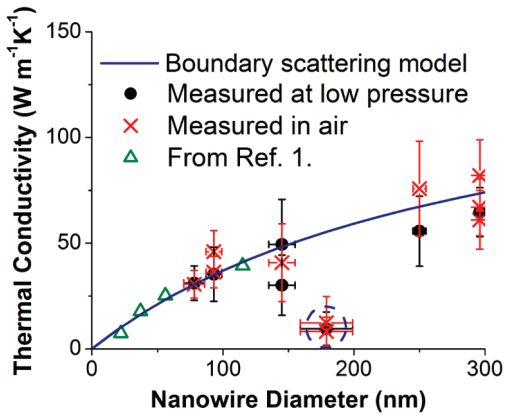

Figure 4. Thermal conductivity measurements for individual Si NWs in air and at low pressure. The predicted curve assuming diffuse boundary scattering is included for comparison, as well as previous experimental data from VLS Si NWs in ref 1.

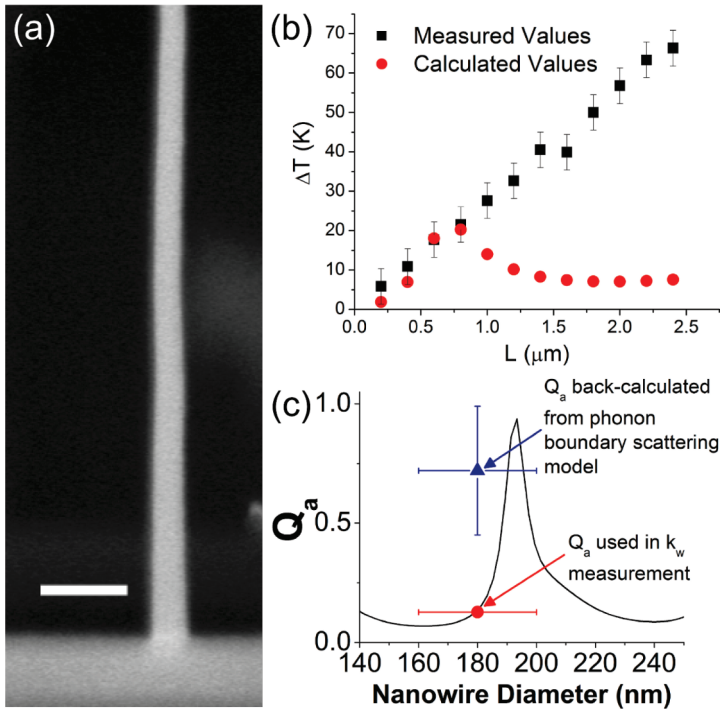

Figure 5. Inverse measurement of the absorption efficiency for an individual highly tapered Si NW. (a) SEM image of the tapered Si NW (scale bar = 500 nm). (b) Experimental ΔT *vs* L for this NW and expected values calculated according to eq 1 but allowing D_w, Q_a, and k_w to vary with L. (c) Comparison of Q_a calculated according to eq 4 with the value back-calculated from the experimental data in (b) using k_w predicted by the phonon boundary scattering model at the mean diameter for the NW shown in (a).

There is reasonable agreement between the measured points and the predicted values.

It is also notable that many of the measurements made in air and those made at low pressure match each other well, although the gaseous mean free path, λ_{mfp} (which is inversely proportional to absolute pressure), is very different in each case. When λ_{mfp} is much larger than the diameter ($\lambda_{mfp}/D \geq 10$), then convection may be understood in terms of individual collisions of gas molecules on the NW surface and its contribution can be calculated according to the kinetic theory of gases.[9] In this regime, convective heat transfer is linearly proportional to the pressure[22,23] and is negligible in comparison to conduction.[12,23] In the other extreme where $\lambda_{mfp}/D \leq 0.1$ (the continuum regime), thermal gradients with a scale on the order of the NW diameter can exist in the surrounding gas ambient, and convection tends to be more significant. Quantitative heat convection is then usually estimated according to empirical correlations. For the transitional regime in which our measurements in air were performed ($\lambda_{mfp}/D \leq 1$), the relative contribution of convection is not always clear. The similarity in NW thermal conductivity values for measurements in air and vacuum suggests that convection is not a major source of error in this measurement. However, other methods of measuring thermal conductivity may be more sensitive than the one presented here, especially if they depend on small, precisely measured temperature differences.

A clear exception to the agreement between the measured data and the boundary scattering model occurs for a diameter of approximately ~180 nm that is circled in Figure 4. A SEM image of this nanowire is shown in Figure 5a. The average diameter was used for estimating the value of the calculated Q_a to apply in determining k_w, but due to an anomalously high taper for this NW, the actual diameter range probed crosses a large absorption resonance, as seen in Figure 5c. To examine this aberrant measurement in more detail, we calculated expected values of ΔT as a function of the L by replacing the average D_w in eq 1 with a value that changes linearly with L as obtained by the measured taper. The value of Q_a is allowed to change as well according to its dependence on D_w in eq 4, and the expected thermal conductivity from eq 6 is used making it diameter-dependent, as well. Thermal contact resistance is neglected as it should only shift the temperature difference at the base.

The resulting values are shown alongside the experimentally measured values in Figure 5b. While the two curves appear to agree near the NW base, the calculated ΔT values quickly fall off before ~1 μm. The decrease in both k_w and D_w over L should increase ΔT, so it is clear that the calculated curve is dominated by the behavior of Q_a. The experimental results then suggest that the NW is absorbing 633 nm wavelength light resonantly. Indeed, with the diameter fixed at the average value of ~180 nm and by using the thermal conductivity from eq 6 at this diameter value, we find that this NW possesses an effective absorption efficiency of approximately $\sim 0.7 \pm 0.3$, close to the resonant maximum of ~0.94, as seen in Figure 5c. We believe that the difference in the mean diameter of this NW from the calculated diameter of the absorption resonance may reflect the inability of this simplified calculation to address absorption in highly tapered NWs. However, previous photocurrent measurements have shown that experimental resonance curves may be shifted and broadened from the calculated Mie resonance values.[3−5] Furthermore, the geometric cross sectional shape may also affect the specific resonant position,[4] so we cannot rule out a shift in resonant behavior from the calculated curve due to the fact that the Si NWs here are not perfect cylinders but rather possess a hexagonal cross section.

While this is a complication with regard to thermal conductivity measurements, it provides an opportunity to directly and quantitatively measure single nanostructure absorption cross sections. In photocurrent measurements, for example, while external quantum efficiency, η_E, is measured, the internal quantum efficiency, η_I, and Q_a are coupled and neither is directly measured.[3,4] Having an independent means of measuring Q_a would make photovoltaic characterization of

nanostructures more complete. The potential to measure the absolute magnitude of absorption cross sections through Raman thermography by techniques such as the one described here may provide a valuable complement to other photovoltaic measurements. In cases where the thermal conductivity of a nanostructure is well-understood but the morphology makes optical absorption estimates unclear, this is especially valuable.

CONCLUSION

In conclusion, we have presented a simple, nondestructive method to measure NW thermal conductivities based on Raman thermography. The method may be expanded to other geometries such as suspended NWs, and the ability to easily select individual NWs or nanotubes to study makes it ideal for the rapid thermal characterization of one-dimensional nanomaterials. Furthermore, the method may be used to quantitatively measure absorption cross sections directly, a convenient capability if applied to axial nanomaterials with nonregular physical cross sections such as sawtooth faceted NWs[24] or branched NWs,[25] with important implications for engineering nanowire-based photovoltaics.[4] The results demonstrated here highlight the great versatility of Raman spectrometry and the indispensible role that it will play in the fast development of technologies that take advantage of the unique size-dependent properties of nanostructures.

EXPERIMENTAL SECTION

Si NWs were synthesized by vapor−liquid−solid (VLS) growth from 50 or 200 nm Au nanoparticle catalysts[26] on the {111} walls of previously fabricated silicon-on-insulator microtrenches.[27] The large height of the trenches (80 μm) makes any Si background signal negligible when collecting Raman spectra from cantilevered NWs. Au agglomeration and ripening leads to a diameter distribution.[28] Though conditions were optimized to minimize NW taper, even very slight tapering gives rise to some error in the measured NW diameters, the implication of which was discussed in the Results and Discussion section. The NW dimensions were measured from SEM images obtained using a Leo 1550 field emission SEM. The diameter error values used in the analysis are obtained from the NW taper in the region probed by the laser spot and are larger than the resolution of this SEM.

Raman spectra were acquired in backscattering configuration using a JYHoriba LabRAM spectrometer at room temperature. The excitation line was provided by a HeNe laser (632.8 nm wavelength) through an Olympus BX41 super long working distance 100× confocal microscope (numerical aperture = 0.6), which produces a 1.27 μm diameter laser spot. The incident laser light was linearly polarized along the NW axes to maximize scattered intensity[6] and simplify the optical absorption calculation. This was achieved by setting a half-wave plate polarizer in the beam path before the sample to zero and aligning the sample such that the NWs would lie along the laboratory axis corresponding to the direction of the electric field polarization. No polarizers were applied to the collected signal. Power at the sample position was controlled by neutral density filters and varied from 0.25 to 2 mW as measured by a hand-held laser power meter. Raman mapping was done using a high-resolution piezoelectric positioning stage (PI P-562.3CD) with a 10 nm minimum step, interfaced with Labspec v.4 software on a personal computer. Steps along the wire axis ranged from 0.2 to 0.5 μm for total probed lengths from 1.2 to 5 μm, while at least six steps each 0.33 or 0.5 μm were taken across each NW axis. In some cases, the wall contact was not actually in the Raman map, which is acceptable since the thermal conductivity measurement does not depend on thermal contact resistance. Raman spectra at each point are the average of at least three measurements with an integration time of 5 s or greater. Some of the measurements were performed with the sample held at pressures less than 10^{-1} Torr using a Linkam THMS350 V vacuum stage (pressure reduced by a mechanical pump) with a ~0.3 mm thick borosilicate glass window attached to the piezoelectric stage.

The line of highest Raman signal intensity along the NW axis direction was used to determine the temperature profile. First-order optical phonon peak positions in Raman spectra taken along the length of NWs were obtained using fitting functions built-in to the LabSpec software specifically for Raman mapping, and a Lorentzian line shape was used. In a few cases, fitting was also performed (again to a Lorentzian line shape) using the Origin software package to check the results from fitting in LabSpec and to obtain estimates of the error in peak position and hence the error in the temperature measured at each point along the wire axis. Conversion of the peak position data to temperature data was accomplished by applying the anharmonic relationship between these two properties, the measurement of which is described elsewhere.[13] Measurements on each NW were initially performed at a conservatively low power and then analyzed to determine if the thermal conductivity data could be extracted. If a clear temperature rise along the NW axis was not observed, the measurement was performed again at a laser power one level higher. Temperature−position slope values were obtained from at least 5 points, though in most cases 7 to 12 points were used.

Acknowledgment. We acknowledge the support of the National Science Foundation, Grant Nos. EEC-0832819 (through the Center of Integrated Nanomechanical Systems) and DMR-0804646.

Supporting Information Available: Mathematica code used to calculate absorption efficiencies, description of the procedure for estimating the window correction factor, and example Raman spectra from the smallest nanowire examined under low pressure. This material is available free of charge *via* the Internet at http://pubs.acs.org.

REFERENCES AND NOTES

1. Li, D. Y.; Wu, Y. Y.; Kim, P.; Shi, L.; Yang, P. D.; Majumdar, A. Thermal Conductivity of Individual Silicon Nanowires. *Appl. Phys. Lett.* **2003**, *83*, 2934–2936.
2. Hochbaum, A. I.; Chen, R. K.; Delgado, R. D.; Liang, W. J.; Garnett, E. C.; Najarian, M.; Majumdar, A.; Yang, P. D. Enhanced Thermoelectric Performance of Rough Silicon Nanowires. *Nature* **2008**, *451*, 163–U5.
3. Cao, L. Y.; White, J. S.; Park, J. S.; Schuller, J. A.; Clemens, B. M.; Brongersma, M. L. Engineering Light Absorption in Semiconductor Nanowire Devices. *Nat. Mater.* **2009**, *8*, 643–647.
4. Cao, L. Y.; Fan, P. Y.; Vasudev, A. P.; White, J. S.; Yu, Z. F.; Cai, W. S.; Schuller, J. A.; Fan, S. H.; Brongersma, M. L. Semiconductor Nanowire Optical Antenna Solar Absorbers. *Nano Lett.* **2010**, *10*, 439–445.
5. Cao, L. Y.; Park, J. S.; Fan, P. Y.; Clemens, B.; Brongersma, M. L. Resonant Ge Nanoantenna Photodetectors. *Nano Lett.* **2010**, *10*, 1229–1233.
6. Frechette, J.; Carraro, C. Diameter-Dependent Modulation and Polarization Anisotropy in Raman Scattering from Individual Nanowires. *Phys. Rev. B* **2006**, *74*, 161404.

7. Cao, L. Y.; Nabet, B.; Spanier, J. E. Enhanced Raman Scattering from Individual Semiconductor Nanocones and Nanowires. *Phys. Rev. Lett.* **2006**, *96*, 157402.
8. Frechette, J.; Carraro, C. Resolving Radial Composition Gradients in Polarized Confocal Raman Spectra of Individual 3C-SiC Nanowires. *J. Am. Chem. Soc.* **2006**, *128*, 14774–14775.
9. Shi, L.; Li, D. Y.; Yu, C. H.; Jang, W. Y.; Kim, D.; Yao, Z.; Kim, P.; Majumdar, A. Measuring Thermal and Thermoelectric Properties of One-Dimensional Nanostructures Using a Microfabricated Device. *J. Heat Transfer* **2003**, *125*, 881–888.
10. Choi, T. Y.; Poulikakos, D.; Tharian, J.; Sennhauser, U. Measurement of the Thermal Conductivity of Individual Carbon Nanotubes by the Four-Point Three-Omega Method. *Nano Lett.* **2006**, *6*, 1589–1593.
11. Balandin, A. A.; Ghosh, S.; Bao, W. Z.; Calizo, I.; Teweldebrhan, D.; Miao, F.; Lau, C. N. Superior Thermal Conductivity of Single-Layer Graphene. *Nano Lett.* **2008**, *8*, 902–907.
12. Hsu, I. K.; Pows, M. T.; Bushmaker, A.; Aykol, M.; Shi, L.; Cronin, S. B. Optical Absorption and Thermal Transport of Individual Suspended Carbon Nanotube Bundles. *Nano Lett.* **2009**, *9*, 590–594.
13. Doerk, G. S.; Carraro, C.; Maboudian, R. Temperature Dependence of Raman Spectra for Individual Silicon Nanowires. *Phys. Rev. B* **2009**, *80*, 073306.
14. Ju, Y. S.; Goodson, K. E. Phonon Scattering in Silicon Films with Thickness of Order 100 nm. *Appl. Phys. Lett.* **1999**, *74*, 3005–3007.
15. Cahill, D. G.; Ford, W. K.; Goodson, K. E.; Mahan, G. D.; Majumdar, A.; Maris, H. J.; Merlin, R.; Phillpot, S. R. Nanoscale Thermal Transport. *J. Appl. Phys.* **2003**, *93*, 793–818.
16. Kerker, M. *The Scattering of Light, and Other Electromagnetic Radiation*; Academic Press: New York, 1969.
17. Sun, B. K.; Xiang, Z.; Grigoropoulos, C. P. Spectral Optical Functions of Silicon in the Range of 1.13−4.96 eV at Elevated Temperatures. *Int. J. Heat Mass Transfer* **1997**, *40*, 1591–1600.
18. Schmid, H.; Bjork, M. T.; Knoch, J.; Riel, H.; Riess, W.; Rice, P.; Topuria, T. Patterned Epitaxial Vapor−Liquid−Solid Growth of Silicon Nanowires on Si(111) Using Silane. *J. Appl. Phys.* **2008**, *103*, 024304.
19. Piscanec, S.; Cantoro, M.; Ferrari, A. C.; Zapien, J. A.; Lifshitz, Y.; Lee, S. T.; Hofmann, S.; Robertson, J. Raman Spectroscopy of Silicon Nanowires. *Phys. Rev. B* **2003**, *68*, 241312.
20. Hsu, I. K.; Kumar, R.; Bushmaker, A.; Cronin, S. B.; Pettes, M. T.; Shi, L.; Brintlinger, T.; Fuhrer, M. S.; *et al.* Optical Measurement of Thermal Transport in Suspended Carbon Nanotubes. *Appl. Phys. Lett.* **2008**, *92*, 063119.
21. Pop, E.; Mann, D. A.; Goodson, K. E.; Dai, H. J. Electrical and Thermal Transport in Metallic Single-Wall Carbon Nanotubes on Insulating Substrates. *J. Appl. Phys.* **2007**, *101*, 093710.
22. Wright, D. R.; Hartman, D. C.; Sridharan, U. C.; Kent, M.; Jasinski, T.; Kang, S. Low Temperature Etch Chuck: Modeling and Experimental Results of Heat Transfer and Wafer Temperature. *J. Vac. Sci. Technol., A* **1992**, *10*, 1065–1070.
23. Piejak, R.; Godyak, V.; Alexandrovich, B.; Tishchenko, N. Surface Temperature and Thermal Balance of Probes Immersed in High Density Plasma. *Plasma Sources Sci. Technol.* **1998**, *7*, 590–598.
24. Doerk, G. S.; Radmilovic, V.; Maboudian, R. Branching Induced Faceting of Si Nanotrees. *Appl. Phys. Lett.* **2010**, *96*, 123117.
25. Doerk, G. S.; Ferralis, N.; Carraro, C.; Maboudian, R. Growth of Branching Si Nanowires Seeded by Au−Si Surface Migration. *J. Mater. Chem.* **2008**, *18*, 5376–5381.
26. Doerk, G. S.; Lestari, G.; Liu, F.; Carraro, C.; Maboudian, R. *Ex Situ* Vapor Phase Boron Doping of Silicon Nanowires Using BBr_3. *Nanoscale* **2010**, *2*, 1165–1170.
27. Gao, D.; He, R. R.; Carraro, C.; Howe, R. T.; Yang, P. D.; Maboudian, R. Selective Growth of Si Nanowire Arrays *via* Galvanic Displacement Processes in Water-in-Oil Microemulsions. *J. Am. Chem. Soc.* **2005**, *127*, 4574–4575.
28. Ferralis, N.; Maboudian, R.; Carraro, C. Structure and Morphology of Annealed Gold Films Galvanically Displaced on the Si(111) Surface. *J. Phys. Chem. C* **2007**, *111*, 7508–7513.